Available online at www.sciencedirect.com
ScienceDirect
ELSEVIER
International Journal of Rock Mechanics & Mining Sciences 45 (2008) 1195–1210
International Journal of Rock Mechanics and Mining Sciences
www.elsevier.com/locate/ijrmms

Consolidation settlements above deep tunnels in fractured crystalline rock: Part 1—Investigations above the Gotthard highway tunnel

C. Zangerl[a,b,*], K.F. Evans[a], E. Eberhardt[a,c], S. Loew[a]

[a]*Engineering Geology, Swiss Federal Institute of Technology (ETH Zurich), Zurich, Switzerland*
[b]*alpS GmbH, Centre for Natural Hazard Management, Grabenweg 3, A-6020 Innsbruck, Austria*
[c]*Geological Engineering/Earth and Ocean Sciences, University of British Columbia, Vancouver, Canada*

Received 4 September 2006; received in revised form 21 January 2008; accepted 14 February 2008
Available online 1 April 2008

Abstract

Surface subsidence associated with tunnelling in fractured crystalline rock masses is rarely considered to be large enough to be a cause for concern. Recent high precision levelling measurements along the Gotthard Pass road in Central Switzerland, however, have revealed up to 12 cm of subsidence along sections that pass several hundred metres above the Gotthard highway tunnel. Large-scale consolidation associated with pore-pressure reduction in the rock mass arising from tunnel drainage is believed to be the contributing mechanism. Although these settlements may appear to be small compared to those associated with groundwater or oil and gas withdrawal from more compliant porous media, they are large enough to adversely affect the structural integrity of sensitive concrete structures on the surface (e.g. thin-arch concrete dams). This is a concern for the 57 km long Gotthard Base Tunnel, which is currently under construction, as it will pass through similar geological conditions as the Gotthard highway tunnel and underneath several important dams. The prediction of the expected settlements requires a more complete understanding of the processes underlying the settlements than exist at present. This paper (Part 1) and a companion paper (Part 2) are a contribution towards this end. In Part 1 we examine the question of consolidation in fractured crystalline rock, introduce the geodetic data and the geological setting of the subsidence associated with the Gotthard highway tunnel. Possible mechanisms for the consolidation are described and estimates obtained for the key hydro-mechanical parameters that govern their action, such as the normal stiffness of fault zones. These data are used to condition analytical scoping calculations of expected subsidence based upon poro-elastic theory, and to provide input for a series of numerical models used to obtain a more detailed understanding of the data, which are presented in Part 2.

Keywords: Consolidation; Fractured rock mass; Tunnel drainage; Subsidence; Coupled hydro-mechanical behaviour; Gotthard tunnel

1. Introduction

In 1998, the Swiss Federal Office of Topography completed a routine high-precision levelling survey over the Gotthard Pass road in central Switzerland. Comparison with the results from a survey over the same route in 1970 revealed that up to 12 cm of subsidence had occurred over a 10 km section that passed several hundred metres above the Gotthard highway tunnel. Comparison between earlier surveys in 1918 and 1970 showed only a steady alpine uplift rate of approximately 1 mm/year. Local surface processes such as landslides could be discounted as the cause of the subsidence because of the scale and the absence of indicators. The coincidence in time and space between the measured settlements and the excavation of the highway tunnel (begun in 1970 and completed in 1977) suggested that the surface deformation was associated with the tunnelling activity, most likely resulting from water drainage from the rock mass into the tunnel. The development of surface settlements over the tunnel was unexpected because it was driven through low-porosity ($\leqslant 1\%$ intact matrix porosity) fractured crystalline rock,

DOI of original article: 10.1016/j.ijrmms.2008.02.005
*Corresponding author at: alpS GmbH, Centre for Natural Hazard Management, Grabenweg 3, A-6020 Innsbruck, Austria.
Tel.: +43 512 392929 14; fax: +43 512 392929 39.
E-mail address: zangerl@alps-gmbh.com (C. Zangerl).

1365-1609/$ - see front matter © 2008 Elsevier Ltd. All rights reserved.
doi:10.1016/j.ijrmms.2008.02.002

whereas significant settlements are more commonly associated with consolidation of high porosity sedimentary rock masses. An extensive field, laboratory and numerical modelling campaign were therefore initiated to understand the processes underlying the observed subsidence [1].

The study was given added importance by plans for the new 57 km AlpTransit Gotthard Base Tunnel, currently under construction, which was approved in 1998 and is expected to be completed in 2016. The possibility of inducing significant surface subsidence is of major concern given the proximity of several concrete dams to the tunnel trajectory (Fig. 1). Thus, there is considerable practical importance to understanding the mechanisms underlying the settlements, so that the risk to surface infrastructure posed by the tunnel construction can be evaluated and remedial measures devised as necessary.

This study consists of two papers. The first presents the results of field measurements from the geological investigation and geodetic campaigns, and introduces the working hypothesis that hydro-mechanically coupled processes relating to rock mass drainage account for the surface deformation processes. Several mechanisms are presented to explain how surface settlements in a crystalline rock mass may be generated when the majority of the draining geological structures are steeply inclined. In the companion paper that follows in this volume (hereafter referred to as Part 2) we evaluate the conceptual models by constructing a series of numerical models, using both discontinuum and continuum techniques, to identify the combined roles that fractures, fault zones and the intact rock matrix may have played in generating the measured settlements following drainage into the Gotthard highway tunnel.

2. Consolidation settlements induced by tunnelling

Consolidation processes resulting from tunnel excavation and groundwater drainage have a history of causing unexpected settlements, and attendant damage to surface structures. Schmidt [2] noted that, in general, tunnel engineers and project managers fail to consider the potential for troublesome subsidence, but that enough cases have now been reported to compile an experience-base to better understand the underlying causes. These cases, however, almost exclusively involve shallow tunnels excavated in soft, unconsolidated soils. The consolidation phenomenon has heretofore not been recognised as important in fractured low-porosity rock, even though large reductions in pore pressure can occur when driving a deep tunnel. Reported instances do exist; however, they are far less numerous than those in soil. Karlsrud and Sander [3] report a case in Oslo, Norway, although in this instance, the fractured bedrock through which the tunnel was driven only provided the drainage network, the consolidation occurring in overlying beds of soft marine clays. A more pertinent example is the case of the Zeuzier arch dam in western Switzerland, where 13 cm of vertical settlement at the dam site was associated with the driving of an investigation adit 1.5 km away through a confined, fractured, marly-limestone aquifer [4,5]. Although these settlements may appear to be small, especially in comparison to those associated with groundwater or oil/gas extraction [6–8], they can nevertheless have serious consequences, since only minor differential displacements are necessary to induce damage in concrete structures. In the Zeuzier case, cracks in the dam appeared which

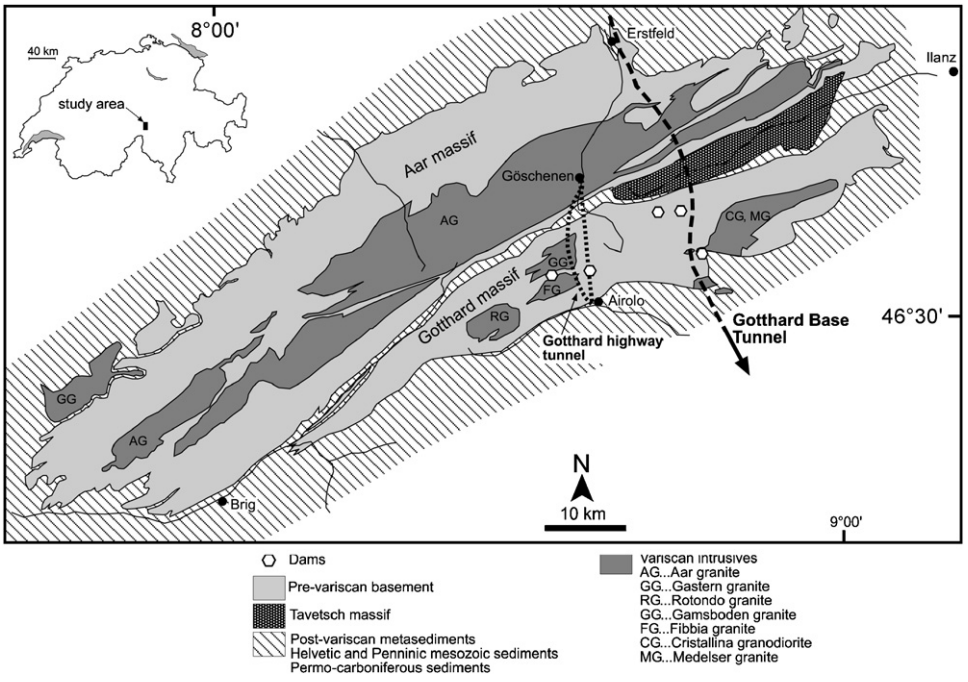

Fig. 1. Geographical and geological setting of the Gotthard massif (after [12]) showing the location of the Gotthard highway and railway tunnels, the Gotthard Base Tunnel that is currently under construction, and the hydroelectric dams in the vicinity of the tunnels.

required the impounded reservoir to be emptied whilst the dam was repaired over a period of several years.

Although the experiences at the Zeuzier dam provide some guidance in investigating the origin of the surface settlements above the Gotthard highway tunnel, an important difference is the nature of the rock masses through which the respective tunnels were driven. The rock mass penetrated by the Gotthard highway tunnel primarily consists of paragneisses and granitic gneisses, and the majority of brittle fault zones and fractures are steeply inclined and strike NE–SW roughly sub-perpendicular to the tunnel axis.

3. Consolidation settlements associated with the Gotthard highway tunnel

The 16.9 km long, two-lane Gotthard highway tunnel was built between 1970 and 1977 to provide a safe, year-round road connection between the northern and southern parts of Switzerland (Fig. 2). The maximum overburden above the tunnel of 1500 m is reached near the Gotthard pass (Fig. 3). During construction, a smaller safety tunnel was driven several hundred meters ahead of and parallel to the primary tunnel. The safety tunnel is located 30 m east of the main tunnel, and has a cross sectional area of between 7 and 10 m^2, as opposed to 69 and 96 m^2 for the main tunnel. A 12–18 month time lag was maintained between the two advancing tunnel faces during excavation. This allowed the safety tunnel to serve both as an investigation and drainage adit.

Other tunnels in the immediate vicinity include the 14.9 km Gotthard (SBB) railway tunnel, located several kilometres east of the highway tunnel. This was built between 1872 and 1881, and has a maximum overburden of 1700 m. Also nearby are two shallow tunnels (maximum overburdens of 150 m) constructed in 1947 to connect the Lucendo and Sella dams with the power station in Airolo (Fig. 2). In addition, the Swiss Army has conducted extensive underground works in the region of the Gotthard Pass. However, information about the exact location and depth of these excavations is not accessible to the public.

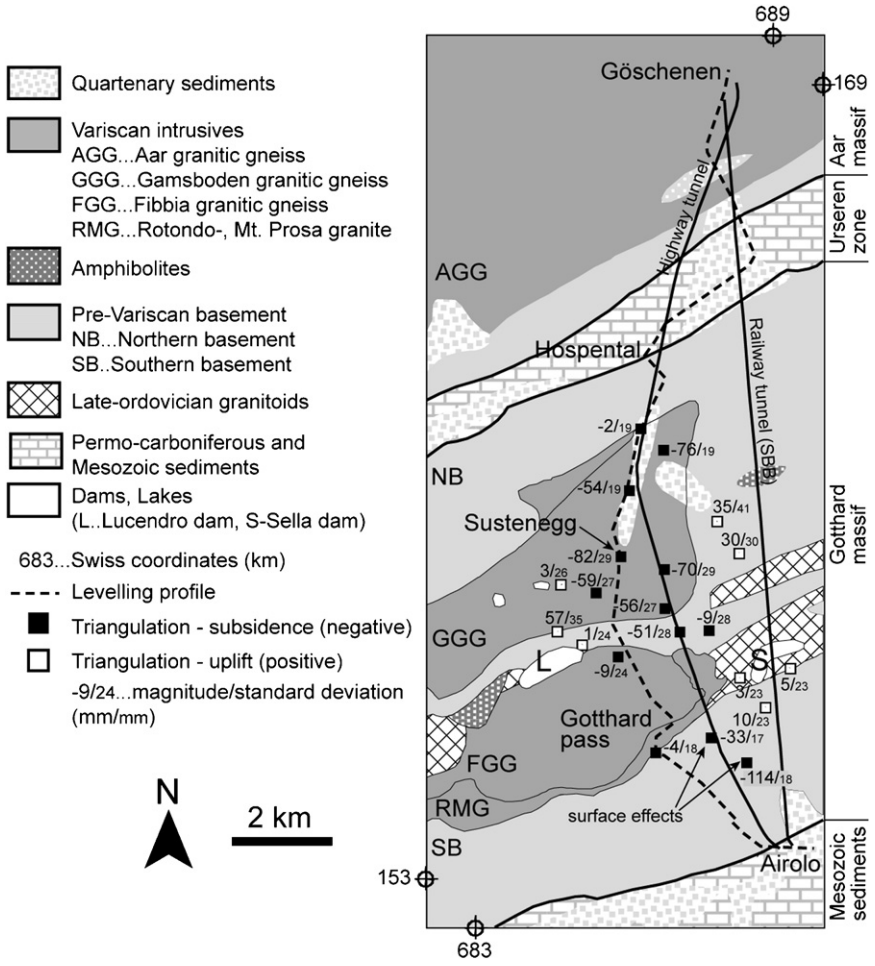

Fig. 2. Geological map of the study area showing the trajectories of the Gotthard A2 highway tunnel (solid line), the local N2 road that goes over the Gotthard pass (dashed line) and the railway tunnel (straight black line). The surface levelling profile follows the Gotthard Pass road. Also marked are the locations of the triangulation survey stations with the estimated magnitude and standard deviation of vertical displacement given in millimetres [11].

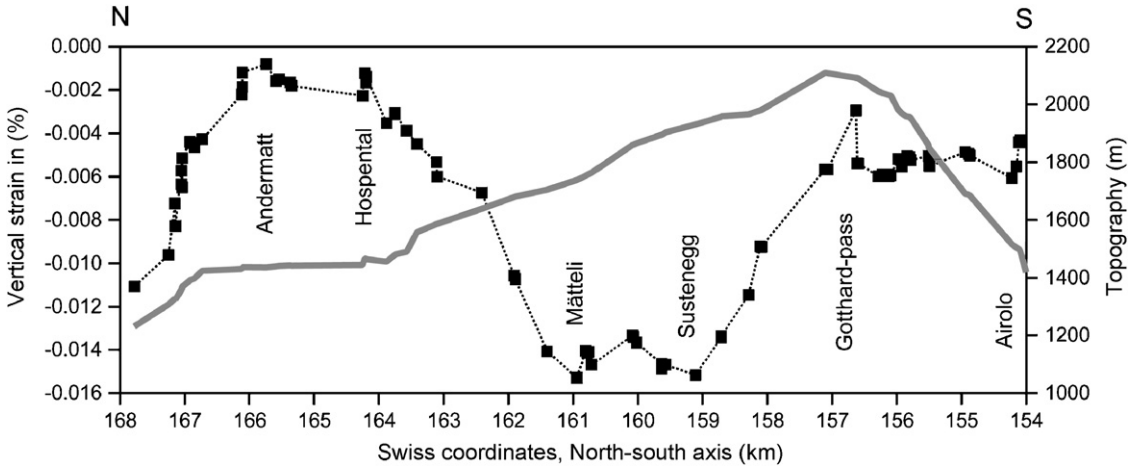

Fig. 3. Topographic profile along the Gotthard Pass road (solid grey line). The irregular dotted line denotes the vertical strain computed from the subsidence profile in Fig. 4a assuming a zero-displacement reference at the level of the tunnel.

3.1. Geodetic data and deformation measurements

The Swiss Federal Office of Topography has carried out high precision levelling measurements since 1903 to establish an official elevation and reference system for Switzerland. Repeat measurement campaigns conducted between 1943 and 1991 were used, amongst other data, to resolve recent crustal movements [9]. Recent levelling campaigns in the region of the Gotthard Pass were carried out in 1993/98. These used closed loops over the Gotthard Pass road and back through both the highway and railway tunnels (unpublished reports: TB 97-40 and TB 98-27). The N–S line over the Gotthard Pass road repeated two earlier campaigns made in 1918 and 1970, prior to highway tunnel construction (Fig. 2). Comparison of the 1918 and 1970 surveys that both pre-date highway tunnel construction revealed the presence of uplift amounting to 1 mm/year, which is thought to be related to the Alpine orogeny. This uplift rate concurs with estimates of 0.75 mm/year obtained using fission–track techniques [10]. In contrast, the surveys made between 1970 and 1993/1998, the period which includes tunnel construction, showed significant downward displacements localised to a 10 km section of the N–S line above the tunnel (Fig. 4a). The maximum subsidence of 12 cm occurs at Sustenegg, and is undoubtedly real since the standard deviation at this point is 4.8 mm.

The validity of the large-scale deformation suggested by the data was assessed by a team of specialists assigned by the Swiss Federal Office of Topography. The levelling data were corrected for the usual sources of error associated with levelling in mountainous terrain, including geoid error and atmospheric refraction. The closure error of the closed profiles after these corrections had been applied were generally less than 2.5 cm. Furthermore, the benchmarks between Hospental and Airolo were inspected and found to be located mostly on either rock outcrops or concrete structures directly in contact with the *in situ* rock mass,

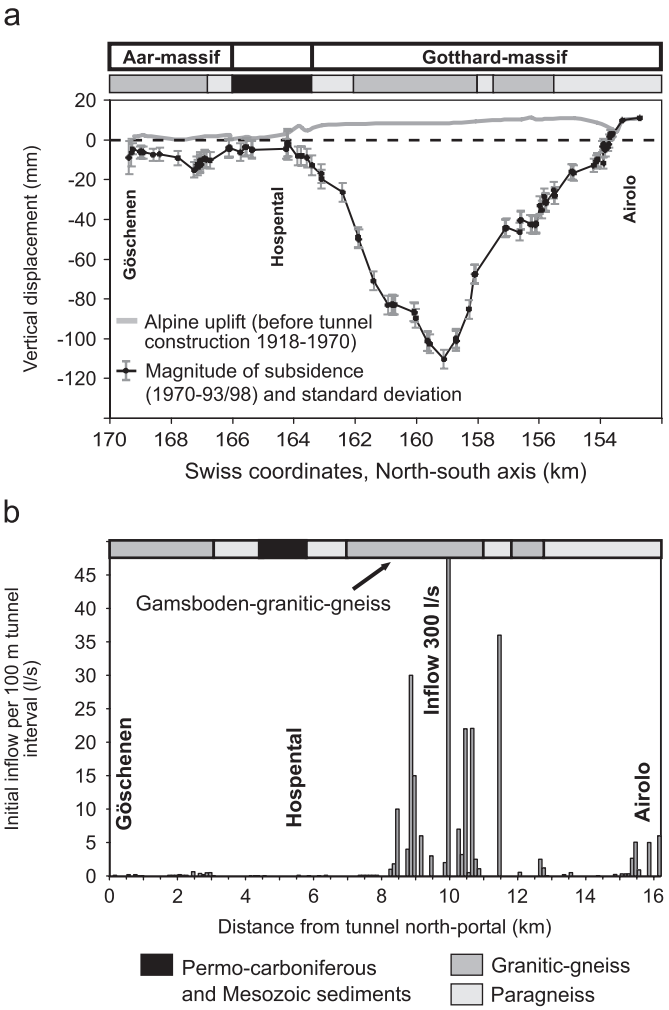

Fig. 4. (a) Results of repeat levelling campaigns along the Gotthard Pass road showing the profiles of surface elevation change for the time intervals 1918–1970 and 1970–1993/98. The former shows the effects of gradual alpine uplift. The latter includes the period of construction of the Gotthard highway tunnel; (b) estimated initial inflow rates into the Gotthard highway safety tunnel per 100 m interval during excavation.

with only a few located on soil cover [1]. Thus, there is no reason to doubt the existence of the subsidence trough.

The existence of the subsidence trough was subsequently confirmed by surface triangulation measurements [11]. These measurements were based on classical triangulation surveys carried out in 1920 and 2000 (i.e. theodolite, tachymeter) supplemented by GPS (global positioning system) data (Fig. 2). Overall, the accuracy of the vertical displacement estimate from triangulation was found to be considerably lower than that from the levelling technique. For example, a standard deviation of 29 mm was calculated for the largest subsidence estimate of 82 mm, which occurred near Sustenegg. However, the triangulation data sets include points outside the zone immediately alongside the Gotthard Pass road (to which the levelling profile measurements were restricted), and thus provide constraints on the lateral extent of the subsidence trough. The estimated subsidence rates at each triangulation station are marked on Fig 2. These show that the extension of the trough in the E–W direction is markedly smaller than that in the N–S direction (note that unfilled square symbols in Fig. 2 indicate uplift). Two triangulation points located at exposed spots southeast from the Gotthard pass show large subsidence magnitudes of 33 and 114 mm (Fig. 2). However, these are believed to be related to surficial mass movements.

The profile of subsidence along the trough does not correlate with overburden or topography. This is shown in Fig. 3 where the topography is plotted with ''vertical strains'' calculated from measured vertical displacements normalised by the distance between surface and the tunnel elevation at specific levelling points. The maximum vertical strain of −0.015% occurs between Mätteli and Sustenegg in the Gamsboden granitic-gneiss, whereas the topography and tunnel overburden reach their maximum at the Gotthard pass, some 2 km to the south, where the vertical strain is only 0.0055%. The absence of a correlation between vertical strain and overburden suggests that surface subsidence is not significantly influenced by topographical effects.

3.2. Geological investigations

The Gotthard massif is situated in the central Swiss Alps (Fig. 1) and covers an area of 580 km^2. It outcrops in the form of an 80 km long and 12 km wide N–E striking mountain range. The study area is located in the central part of the massif through which the Gotthard highway and rail tunnels penetrate. Both tunnels pass through the tectonic units of the Aar massif, the Urseren zone, the Gotthard massif and Mesozoic cover sediments (Fig. 2). The Aar and Gotthard massifs are an uplifted part of the European crust. Labhart [12] describes these massifs as representing a poly-orogenic and poly-metamorphic crystalline basement (''Altkristallin'') made up of paragneisses, amphibolites, migmatites, migmatic gneisses, late-Ordovician granites and middle-Palaeozoic metasediments, intruded by late-Variscian plutons (the Aar, Gamsboden and Fibbia granites). These rock bodies were overprinted by alpine metamorphism, mostly in greenschist facies. The alpine deformation is characterised by the development of a NE–SW striking main foliation. Throughout these massifs, brittle and ductile alpine fault zones showing a NE–SW, NNE–SSW or WNW–ESE strike can be found.

The first stage of the field campaign involved the mapping of brittle fault zones on a regional scale in the area between Hospental and Airolo (Fig. 2). The diverse spatial properties exhibited by brittle fault zones relative to single fractures, especially with respect to their size and properties, required that they be treated and evaluated independently. The mapping of the brittle fault zones included the sampling of internal fracture orientations, their structural architecture, and their relationship to foliation, meso-scale structures (i.e. extensional joints and shear fractures on scales of 1–10 m) and geological boundaries [13]. A 2-D trace map of brittle fault zones in the Gamsboden granitic-gneiss derived from field mapping and aerial photos is presented in Fig. 5. The poles to brittle fault zones mapped on the walls of the highway safety tunnel [14,15] and on surface outcrops are shown in the stereographic plots of Figs. 6a and b, respectively. Almost all brittle fault zones are steeply inclined and in a clockwise sense strike between NNE–SSW and WNW–ESE. They are also sub-parallel to the foliation, geological boundaries, ductile fault zones and meso-scale fractures, all of which define a fan-like structure of NE–SW strike (Fig. 7; see also [13]). A total of 294 brittle fault zones were found along the safety tunnel between Hospental and Airolo [16]. Their spatial distribution was found to fit a negative exponential probability distribution with a mean total spacing of 35 m [13]. For the section within the Gamsboden granitic-gneiss, the mean total spacing was 35.6 m, with minimum and maximum total spacing of 1 and 178 m, respectively. Meso-scale fractures complement the large-scale fault zones in completing the discontinuity network (stereonet plots in Fig. 7). These meso-scale fractures were mapped on random outcrops along the Gotthard Pass road and within unlined sections of the Gotthard safety tunnel. Detailed scanline mapping was also carried out along sections of interest. The outcrop mapping focussed on determining fracture orientation, surface structure, abutment relationships between individual fracture sets and fracture infilling. The more systematic scanline mapping allowed fracture size, spacing and frequency to be measured. Probability distributions describing these geometrical parameters were used to constrain the 2-D fracture network model that formed the basis of the discrete-element modelling presented in Part 2. Geological, structural and topographical data were collected and managed through a GIS database, which was subsequently programmed to resolve the orientations and spatial relationships between dominant joint sets. The statistical treatment and characterisation of these data sets are described in more detail in [13].

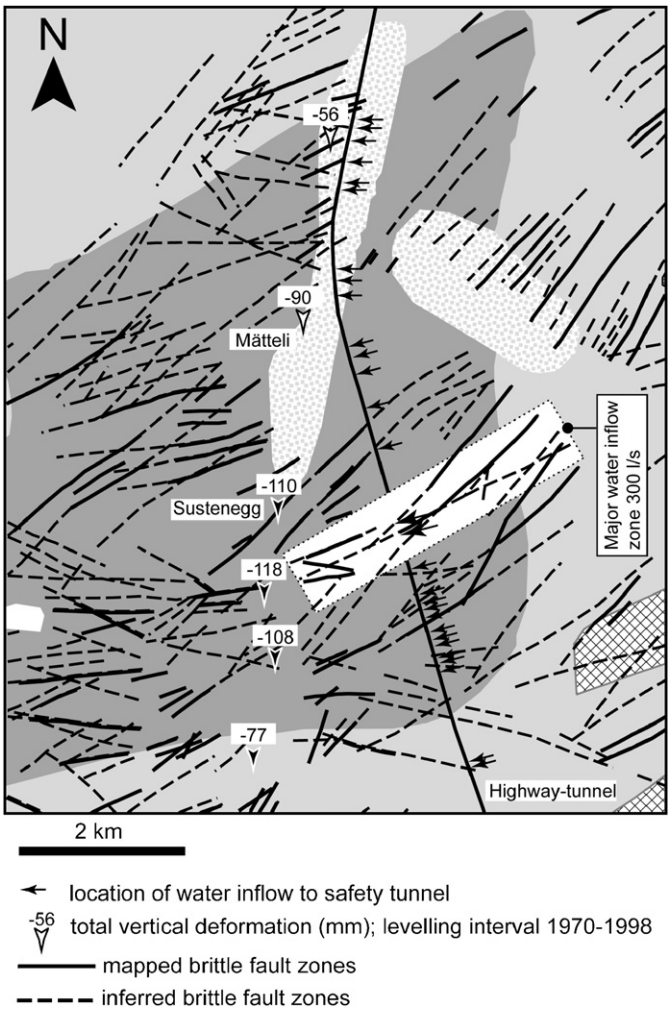

Fig. 5. Map of the extent of the Gamsboden granitic gneiss showing the traces of inferred (from air photos) and mapped fault zones. The trajectory of the Gotthard highway tunnel is shown by the solid line, with the location of major tunnel inflow zones denoted by the arrows. The village of Hospental is situated immediately to the north of the map, and Airolo immediately to the south (see Fig. 2). The numbers in white boxes refer to subsidence between 1970 and 1998 at levelling survey stations.

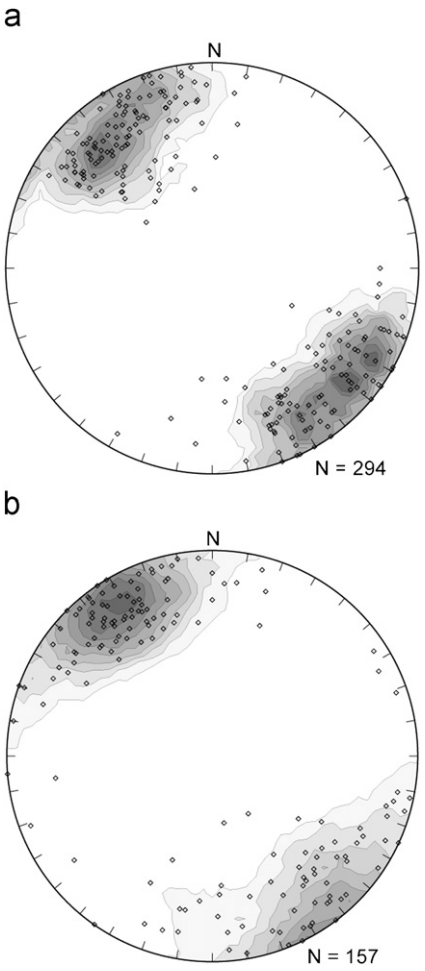

Fig. 6. Stereographic plots of brittle fault zones mapped: (a) within the Gotthard safety tunnel; (b) on surface. The data are plotted using equal-area Kamb-contour pole plots projected onto the lower-hemisphere.

The results of outcrop and tunnel mapping of the meso-scale fractures within the Gamsboden granitic-gneiss are summarised in Table 1 and Fig. 7. Four distinct fracture sets are recognised, and all are found on both the surface and the tunnel exposures, implying they extend to depths of at least 500 m. However, their mean normal-set spacing varies with depth, with a higher fracture frequency being found near the surface (Fig. 8). The *in situ* block size distribution (ISBD, after [17]) was estimated using the empirical approach proposed by Lu and Latham [18]. This was applied to the surface and tunnel data sets of meso-scale fractures (Table 1) consisting of fracture sets #1, #2, and a set formed by combining sets #3 and #4. The fracture spacing distributions for the three sets were approximated by a negative exponential distribution function as illustrated in Fig. 8 for fracture set #1. The resulting block size distributions are shown in Fig. 9. The estimated volume of the largest blocks approaches 1000 m^3 at the tunnel level but is less than 30 m^3 at surface. The corresponding maximum block lengths, assuming cubic block shapes, are 10 m and 3 m, respectively.

3.3. Hydrogeological investigation and tunnel inflows

As noted earlier, during construction of the Gotthard highway tunnel, a safety tunnel was excavated several hundred meters ahead of the primary tunnel. The locations where water bearing fractures were intersected and the estimated initial inflow rates are shown in Figs. 4b and 7. The inflow estimates are coarse and not derived from instrumentation [14,15]. Nevertheless, it is evident that zones of inflow were primarily encountered in the Gamsboden granitic-gneiss. The highest initial net inflow estimated as approximately 300 l/s occurred over a 100 m section that included two brittle fault zones, 23 m apart, near Tunnel Metre (TM measured from the north portal) 9910 and 9933 (Fig. 4b), and was associated with a strong geothermal anomaly. These fault zones, which have widths of 19 and 14 m, are estimated to have initially contributed

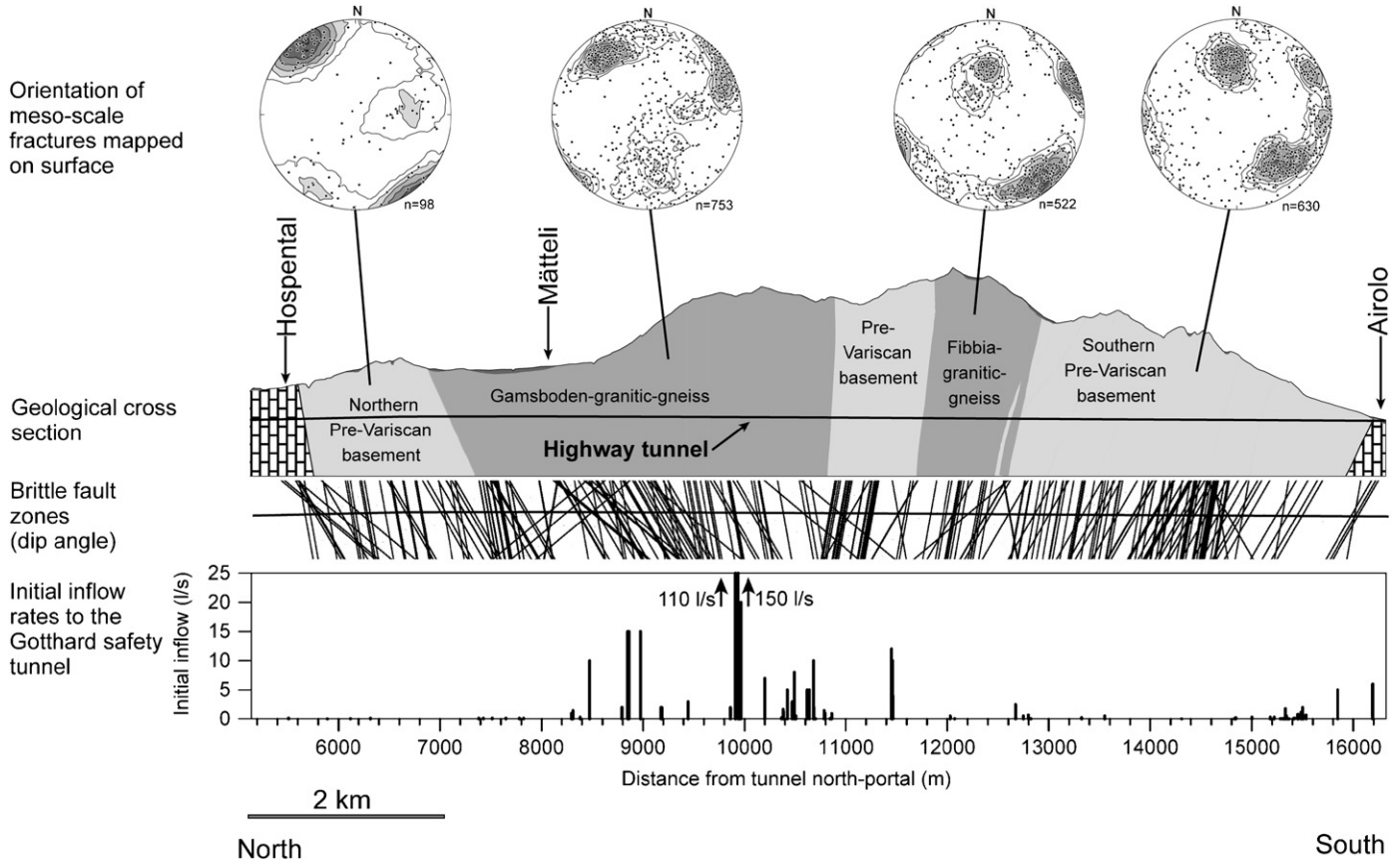

Fig. 7. Geological and structural cross sections showing the main geological units and brittle fault zones mapped within the Gotthard highway safety tunnel. The stereoplots above (lower hemisphere) show poles to meso-scale fractures mapped on the surface above the tunnel in each of the main geological units. The frame at the bottom shows the location and estimated initial rate of inflow of water-bearing fault zones intersected along the safety tunnel.

Table 1
Orientation and spacing of meso-scale fractures within the Gamsboden granitic-gneiss based on scanline mapping

Location	Fracture set #	Mean dip direction/ dip angle (°)	k^*	θ^* (°)	Discontinuities mapped	Mean spacing (m)	Standard deviation (m)
Surface data	1	137/71	21.7	1.5	461	0.47	0.65
	2	222/87	1.3	18.3	217	1.31	2.84
	3	352/61	13.8	2.4	280	0.91	1.75
	4	264/40	9.7	5.9	67	0.90	1.32
Tunnel data	1	138/74	32.1	2.9	169	1.68	3.84
	2	236/80	37.7	5.4	20	No data	No data
	3	1/60	14.0	5.5	159	0.79	1.36
	4	257/43	24.8	4.3	46	>3 estimated	No data

*Precision, k, and apical half-angle, θ of 95%-confidence cone from Fisher analysis.

150 and 110 l/s to the net inflow, and had estimated hydraulic transmissivities of 2.6e-4 m^2/s and 2.2e-4 m^2/s, respectively [19]. The transmissivities were inferred from the initial inflow estimates through application of a constant head solution for 2-D transient, radial flow in confined aquifers whose widths correspond to the width of the fault zones [20]. Today, a net steady-state inflow rate of 8 l/s is measured from this 100 m tunnel interval.

A variety of data indicate that the high-transmissivity fault zones are largely restricted to granitic rock. It is evident from Fig. 4b that zones of high inflow occur only in competent granitoid rock, principally the Gamsboden granite, the inflows observed in the schistose paragneisses to the north and south of the granitic gneisses being several orders of magnitude lower. An exception is the paragneissic rock unit that lies between the Gamsboden and

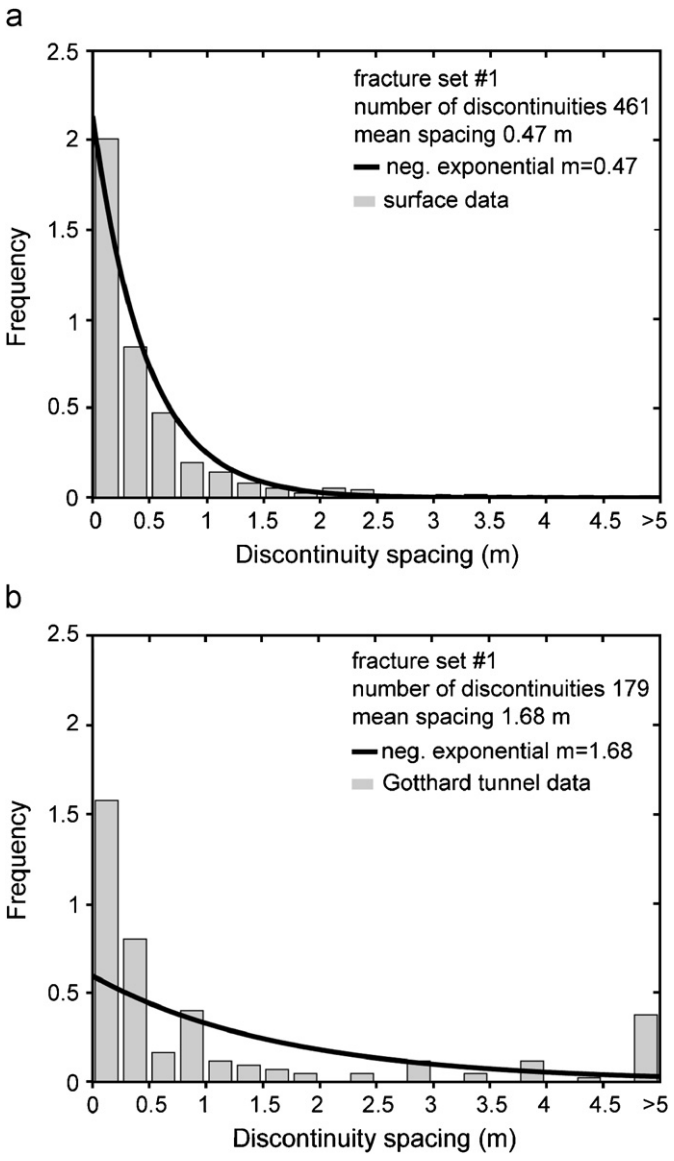

Fig. 8. Normal set spacing distribution of set #1 (see Table 1) of the meso-scale fractures within the Gamsboden granitic gneiss, measured: (a) on surface; and (b) from the Gotthard highway safety tunnel.

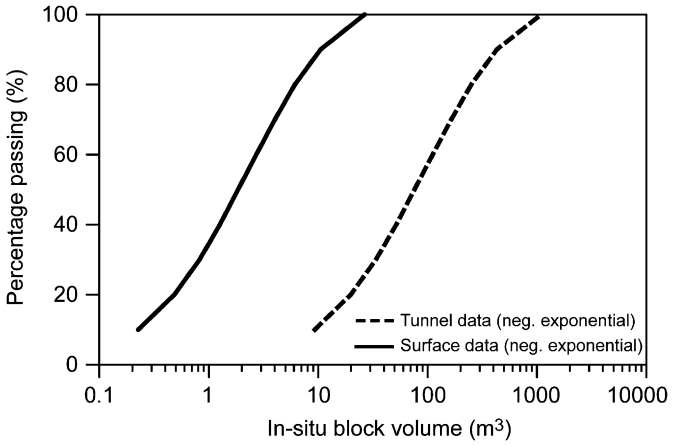

Fig. 9. *In situ* block size (volume) distribution calculated from mapped joint sets on surface and within the Gotthard highway safety tunnel.

Fibbia granitic gneisses which contains a major inflow zone. From Fig. 2 it can be seen that a transition from the Gamsboden gneiss to a paragneiss occurs about 1.5 km east of the highway tunnel. The Gotthard rail tunnel was driven through the paragneiss, which perhaps explains why it did not encounter substantial inflows when crossing these same structures several decades earlier.

The triangulation data indicate that the subsidence trough does not extend more than 2 km to either side of the highway tunnel [11]. If the subsidence reflects drainage-induced pore-pressure drawdown within the rock mass, as discussed shortly, then the narrow E–W extent of the trough would imply that the disturbance did not penetrate more than a couple of kilometres along the strike of the brittle fault zones. A number of factors might plausibly account for this, such as the finite lateral extent of the fault zones, their connectivity, or internal transmissivity heterogeneity. The boundary between the Gamsboden granitic gneiss and the paragneisses some 1.5 km east of the highway tunnel might control the limits of pore-pressure drawdown penetration to the east. Penetration of drawdown to the west may be inhibited by the occurrence of lakes and gravel aquifers on top of the crystalline basement which serve as large storage zones (e.g. the gravel-filled deep trough in the Urseren Valley near Hospental; see Fig. 2).

The widths of the highly transmissive fault zones at TM 9910 and 9933 suggest that they extend to the surface. However, no clearly associated geomorphical features and lineaments could be identified on aerial photos. If they do indeed extend to the surface, and maintain the same uniform transmissivity as they display locally near the tunnel, then locally strong drawdown of the water table might be expected near their surface expression. Spring line mapping on the surface above the central section of the highway tunnel in 2000 showed that most springs occur at a relatively constant altitude of between 2200 and 2500 m a.s.l. In the vicinity of the expected outcrop of the two highly transmissive brittle fault zones, the spring line is relatively well defined at 2200–2300 m. Although the precise level of the spring line prior to tunnel excavation is not known, the present "normal" level suggests that no large drop in water table has occurred as a consequence of tunnel construction. This observation is not consistent with the presence of a simple, uniformly transmissive, planar structure connecting the tunnel to the surface [21]. Rather, it suggests that the highly-transmissive fault zones intersected by the tunnel have a permeability structure which is spatially strongly variable so that the high transmissivity properties seen near the tunnel do not extend to the surface.

The water currently produced by the high-transmissivity fault zones at TM 9910 and 9933 has a relatively high temperature and is low in tritium, indicating that it is mostly old water that is flowing upwards into the tunnel

through the fault zone extension below [19]. This further supports the view that the high transmissivity of the fault zones seen at the tunnel level does not extend continuously to the surface. As such, the permeable fault zones, with their pronounced contrast in conductivity with respect to the matrix rock, would act as a regional sink with considerable lateral extent. The opening of the tunnel would serve to increase the head gradient towards the major fault zones.

4. Possible consolidation mechanisms

The fractured nature of the crystalline rock mass that apparently experienced consolidation, together with the role brittle fault zones played in forming major conduits for tunnel inflows, suggests the working hypothesis that the measured surface subsidence was in part a consequence of closure of fractures in response to reduced pore-pressure (Fig. 10). Reduced pore pressure in the discontinuities would in turn lead to drawdown of pore pressure within the intact rock blocks since these contain significant connected porosity due to the presence of micro-fractures and internal fractures whose scale is smaller than the block size. As a simplification, the drawdown process can be considered to proceed on two time scales: an initially rapid penetration of drawdown along the more permeable structures in the rock mass, such as brittle fault zones and meso-scale fractures, succeeded by slower penetration into the relatively impermeable, intact rock blocks that the fractures bound (Fig. 10). Since the brittle fault zones/fractures and the intact blocks are characterised by different time constants, reflecting different geometrical, mechanical and hydraulic behaviour, they were treated separately to study their mechanical response to pore-pressure drawdown.

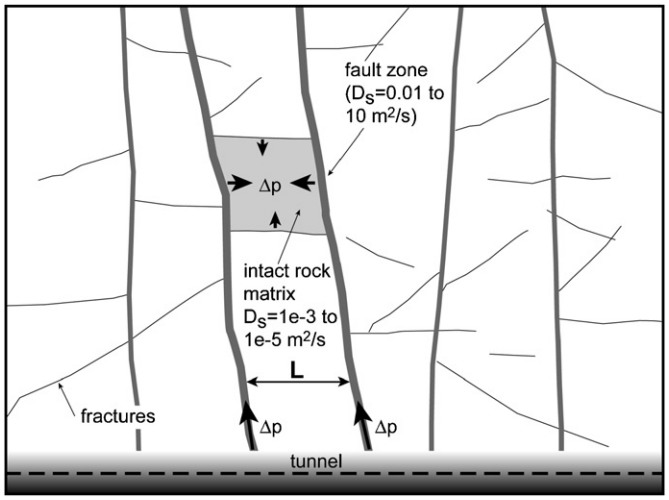

Fig. 10. Conceptual model of diffusion into the "intact blocks" of the fractured crystalline rock. Diffusion takes place into the blocks from the faces of the sub-parallel fault zones and is assisted by more rapid penetration along the meso-scale fractures.

4.1. Coupled hydro-mechanical behaviour of discontinuities

Upon breaching of a conductive fault zone during tunnel excavation, the resulting pore-pressure drawdown in the zone would subsequently produce drainage of the surrounding interconnected discontinuity network, thereby altering their effective stress states and leading to fracture closure. This change in mechanical aperture due to a drop in pore pressure is expressed through the effective stress law for fracture closure:

$$\Delta\sigma'_{\mathrm{n}} = \Delta\sigma_{\mathrm{n}} - \alpha_{\mathrm{f}}\Delta p \tag{1}$$

where σ'_{n} is the effective normal stress, σ_{n} is the total normal stress, α_{f} is the effective stress coefficient and Δp is the pore-pressure change [22]. The change in the effective normal stress acting across a compliant fracture would lead to a change in mechanical aperture, Δa_{m}, given by

$$\Delta a_{\mathrm{m}} = -\frac{\Delta\sigma'_{\mathrm{n}}}{k_{\mathrm{n}}} \tag{2}$$

where $\Delta\sigma'_{\mathrm{n}}$ is the change in effective normal stress, and k_{n} is the normal stiffness at the stress level in question.

Intuitively, the frequency and normal stiffness of sub-horizontal fractures would have the largest impact on surface subsidence as closure of these fractures would directly contribute to vertical settlement. However, given that most of the conductive structures in the Gotthard region are steeply inclined (i.e. the brittle fault zones in Figs. 6 and 7), closure of these structures would generate subsidence only indirectly through a Poisson ratio effect, as discussed in more detail in [16].

The redistribution of total stress arising from fracture closure will generate shear stresses within the rock mass. These may become large enough to produce slip along the numerous steeply inclined fractures and faults within the rock mass. Initial, small, shear displacements are governed by an elastic mechanism, but larger displacements increasingly involve plastic-like slip behaviour. The magnitude of elastic shear displacement, Δs_{e}, which occurs across a fracture subject to a shear stress change, $\Delta\tau$, is described by

$$\Delta s_{\mathrm{e}} = \frac{\Delta\tau}{k_{\mathrm{s}}} \tag{3}$$

where k_{s} is the shear stiffness. The latter is commonly assumed to be either a constant or to be dependent upon the prevailing normal stress on the fracture [23,24]. In general, shear deformation parameters are influenced by scale-effects and surface conditions along the shearing planes. The threshold for the change from purely elastic to plastic shear deformation with increasing shear displacement can be described in its simplest form by the Coulomb effective stress failure criterion given by

$$\tau_{\mathrm{f}} = c + \sigma'_{\mathrm{n}}\ \tan(\phi) \tag{4}$$

where the peak shear stress, τ_{f}, is generally a function of the effective normal stress, σ'_{n}, cohesion, c, and friction angle, ϕ. Thus, the shear stress increase accompanying the initial

elastic shear deformation (itself driven by shear stress increase) is limited at the level of τ_f, the fault shearing irreversibly to prevent the limit being exceeded. This is an approximation since in reality the shear strength of fractures and faults may undergo complex changes during slip due to asperity interactions and damage processes (e.g. [25]).

Fractures deformed in shear under constant normal stress generally dilate due to the effect of asperities overriding one another, resulting in an aperture increase. Under confined conditions (i.e. stiff system boundaries), dilation will be partly suppressed resulting in an increase in normal stress. Shearing thus alters both the aperture and the normal stress acting on the fractures, and hence modifies their mechanical and hydraulic properties (e.g. [26,27]). Dilation is primarily controlled by the roughness and the surface strength of the fracture and the normal stress acting across it.

Changes in mechanical aperture described by Eqs. (1) and (2) generally result in a change in the hydraulic transmissivity of the fracture. If the flow is laminar, this aperture-flow coupling can be approximated by the cubic law equation for flow between two smooth, parallel plates of separation, a_h, given by

$$Q = \frac{\rho g a_h^3}{12\mu} w \nabla p \tag{5}$$

where Q is volumetric flow rate, ρ is fluid density, g is gravitational acceleration constant, μ is dynamic viscosity of the fluid, ∇p is hydraulic gradient in the plane of the fracture and w is fracture breadth perpendicular to the direction of flow. The parameter a_h is referred to as the hydraulic aperture of a fracture. This physically represents the equivalent smooth parallel-plate aperture that would give the same throughput of fluid under the same pressure gradient, and thus can be calculated through flow tests. Hydraulic aperture is generally smaller than the mechanical aperture, a_m (here taken as the arithmetic mean aperture) due to roughness effects [28,29].

4.2. Coupled hydro-mechanical behaviour of the intact rock matrix

The long-term reduction of the pore pressure within intact blocks due to tunnel drainage will result in a consolidation of the blocks. This will modify the stresses acting on the bounding fractures and hence affect their aperture. The hydro-mechanical coupling between pore-pressure drawdown and deformation of the intact blocks can be described by the theory of poroelasticity (i.e. Biot's 3-D consolidation theory [30]). Within this framework, the intact rock blocks are represented as permeable, linear elastic, isotropic, homogeneous porous materials for which the effective stress law in incremental form for elastic deformation is given by

$$\Delta\sigma'_{ij} = \Delta\sigma_{ij} - \alpha\Delta p\delta_{ij} \tag{6}$$

Here, σ'_{ij} is effective stress for elastic deformation, σ_{ij} is total stress, α is the Biot's coefficient, p is pore pressure, and δ_{ij} is the Kroenecker's delta [31]. Biot's coefficient describes the fraction of pore-pressure change that is felt by the solid skeleton as a deforming volumetric body force, and takes values ranging from 0 to 1 [32]. Block deformation resulting from pore-pressure change can be obtained from the poro-elastic stress-strain relations given by [33]

$$\varepsilon_{ij} = \frac{1}{2G}\left[\sigma_{ij} - \frac{v}{1+v}\sigma_{kk}\delta_{ij}\right] + \frac{\alpha}{3K}p\delta_{ij} \tag{7}$$

where ε_{ij} is the macroscopic strain, σ_{kk} is the first stress invariant (i.e. $\sigma_{xx}+\sigma_{yy}+\sigma_{zz}$), G is the shear modulus, K is the drained bulk modulus and v is the drained Poisson's ratio.

The flow and elastic fields are coupled such that changes in pore pressure produce volume deformation, and changes in volume deformation produce changes in diffusivity through its effect on the specific storage coefficient. The effect of volume deformation on permeability is not considered. Conservation of fluid mass gives the time dependent consolidation relationship [33]:

$$\alpha\frac{\partial\varepsilon_v}{\partial t} + S_s|_{\varepsilon=0}\frac{\partial p}{\partial t} = \frac{k}{\mu}\nabla^2 p + Q \tag{8}$$

where ε_v is the volumetric strain, k is the permeability, Q is an explicit fluid source, and $S_{s|\varepsilon=0}$ is the specific storage coefficient of the medium under zero macroscopic strain conditions (see Eq. (14a)).

5. Quantitative considerations of pore-pressure depletion around tunnels

The levelling measurements that revealed the subsidence trough were conducted 20 years after the construction of the Gotthard highway tunnel. Unfortunately there are no data that constrain the development of the trough within this period. As noted earlier, trough subsidence is likely to be controlled by processes that act at two different timescales: At short timescales, by the rate of penetration of pore-pressure drawdown along fault zones intersected by the safety tunnel; and at longer timescales by diffusion of the drawdown from the faces of the fault zones into the rock mass in a direction parallel to the tunnel axis. The latter will involve diffusion along the meso-scale fractures and into the blocks they bound, a process that will generally be expected to be slower, but is no less important because of the much larger rock volume that is affected. In the following, we attempt to place bounds on the time constants involved in the processes using constraints from rock mass hydraulic and mechanical parameters, and data from analogous situations. We then evaluate the magnitude of subsidence that is likely to result from the elastic consolidation mechanisms described earlier.

5.1. Pore-pressure diffusion within the fault zones

An upper-bound on the time, t, required for the effect of tunnel drainage to reach the surface through pore-pressure diffusion along a fault zone can be computed from the relation [34]

$$t = \frac{r^2}{2.25 D_f} \tag{9}$$

where r is the radius of the affected area around the tunnel (i.e. the depth of the tunnel), and D_f is the diffusion constant for the fault zone given by

$$D_f = \frac{T}{S} \tag{10}$$

Here T is the transmissivity of the fault zone and S is the storativity. Eq. (9) is based on radial diffusion through the fault zone from the drained tunnel (i.e. representing a zero pore-pressure boundary). The time constant can be estimated by ascribing values to the transmissivity and storage.

The transmissivities of the permeable brittle fault zones encountered along the Gotthard safety tunnel, mostly within the Gamsboden unit, generally lie within the range 3×10^{-7}–$2.6 \times 10^{-4}\,m^2/s$ [19]. Transmissivity estimates of $1 \times 10^{-5}\,m^2/s$ were found for a 120 m wide fault zone intersecting a tunnel in the nearby Rotondo granite (Fig. 1) [35]. The zone is similar to those intersected in the Gotthard highway safety tunnel inasmuch as it strikes NE–SW and comprises several narrow discrete faults with sections of densely fractured rock in between.

The storativity, S, of a fracture or fault zone is related to its hydraulic aperture, a_h, and normal stiffness, k_n, by [36]

$$S = \rho_f g \left(\frac{a_h}{K_f} + \frac{1}{k_n} \right) \tag{11}$$

where ρ_f is fluid density, g is the gravitational acceleration, and K_f is the bulk modulus of the fluid. The first term in brackets is due to fluid compressibility, and the second reflects volume changes due to fracture aperture changes. The latter term dominates the storativity for all but the stiffest of fractures. This is unfortunate since normal stiffness is difficult to constrain, particularly for well-developed, brittle fault zones of the type encountered in the Gotthard safety tunnel, which are commonly composed of many smaller-scale fractures that often contain thick deposits of fault gouge. In Appendix A we derive an estimate for the normal stiffness of these fault zones using laboratory measurements of the stiffness of gouge and published values of the normal stiffness of unfilled single fractures, which are compiled in [37]. Normal stiffnesses in the range 0.5–30 MPa/mm are found to be reasonable. The storativities of the fault zones implied by these values, obtained from Eq. (11) neglecting the term a_h/K_f, are 2×10^{-5} to 3×10^{-7} m/m, with higher values in the range being considered more appropriate [21]. There are no published storativity estimates for comparable fault zones that we are aware of. Rutqvist et al. [38] estimated the storativity of a single fracture in granitic rock by modelling multi-pressure injection tests and found values in the range 1×10^{-8}–3.3×10^{-7} m/m. These lie near the lower range of our estimates, as expected given that it applies to a single fracture.

Using a range of transmissivities of 3×10^{-7}–$2.6 \times 10^{-4}\,m^2/s$, and storativities of 2×10^{-5}–3×10^{-7} m/m, Eq. (10) yields estimates for diffusivity of 0.02–867 m^2/s. The higher values are considered unlikely since they correspond to the physically unfavoured combination of high transmissivity and low storativity. A more plausible range for the diffusivity of fault zones is 0.02–10 m^2/s. A diffusivity of 0.12 m^2/s was determined between two boreholes drilled in fractured crystalline rock, 250 m apart at the KTB-test site in Germany [39].

Adopting the diffusivity range of 0.02–10 m^2/s for the fault zones, the maximum time span required for the drawdown front to extend to the surface, 800 m above the tunnel, was estimated to be in the range of 8 hours to 165 days (Table 2).

5.2. Pore-pressure diffusion within the intact rock matrix

The drawdown in pressure within the fault zones will not only propagate along the fault, but will also penetrate into the rock mass. This penetration will occur principally along the meso-scale fractures at rates that are significantly slower than within the fault zones. As a consequence, saturated low-permeability intact rock blocks bounded by the fractures would be obliged to adjust their internal pore pressure to maintain equilibrium at their boundaries (Fig. 10). The time required for significant pressure drawdown to penetrate the blocks was estimated by considering the problem of linear diffusion into the blocks from two parallel faces a distance L apart, which represents the block-size. For this geometry, the time required for pore pressures at the mid-point to be drawn down to 90% of the applied drawdown, $t_{90\%}$, is given by [40]

$$t_{90\%} = \frac{1.03(L/2)^2}{D_i} \tag{12}$$

Table 2
Time (t) required for pore-pressure drawdown within the brittle fault zones of the discontinuity to reach the surface 800 m above the Gotthard highway tunnel

Dimension of fracture network (m)	D_f (m^2/s)	t (d)
$L = 800$	0.02	164.6
$L = 800$	0.1	32.9
$L = 800$	1	3.3
$L = 800$	10	0.3

The diffusion is assumed to be radial, and to occur within a porous material of diffusivity D_f within the fault zone.

where D_i is the diffusion coefficient for the intact rock matrix, which is defined by

$$D_i = \frac{\kappa_i}{S_{si}} \tag{13}$$

where κ_i is the isotropic hydraulic conductivity of the blocks and S_{si} is the corresponding coefficient of specific storage.

No permeability measurements are available for the Gamsboden granitic-gneiss, which is unfortunate since granite permeability can vary over more than four orders of magnitude [41]. The closest rock to the Gamsboden, both geographically and mineralogically, for which matrix permeability information is available is the Aar granite at the Grimsel Rock Laboratory. Vomvoris et al. [42] summarise a variety of *in situ* tests and suggest a matrix conductivity of 3×10^{-12}–2×10^{-10} m/s, with higher values being found near disturbed structures such as faults. Thus we adopt this range as appropriate for scoping calculations. The specific storage coefficient appropriate for intact blocks of the Gamsboden has also not been measured and thus is coarsely estimated by analogy with values for granites of similar porosity. The specific storage coefficient of intact rock includes both a fluid compressibility component scaled by porosity, and an elastic, pore-volume change component determined by poro-elastic constants and dependent upon boundary conditions. For the two extreme boundary conditions of zero strain and zero stress change, the specific storage coefficient (units of m^{-1}) can be written as

$$S_{si}|_{\varepsilon=0} = \rho_f g\left(\frac{n}{K_f} + \left[\frac{\alpha}{K_i} - \frac{n}{K_i}\right]\right) \tag{14a}$$

for zero macroscopic strain (modified after [33]), and

$$S_{si}|_{\sigma_m=0} = \rho_f g\left(\frac{n}{K_f} + \left[\frac{\alpha}{K} - \frac{n}{K_i}\right]\right) \tag{14b}$$

for constant octahedral normal stress, σ_m (modified after [43]). Here, ρ_f is the fluid density, g is the gravitational acceleration, n is the porosity, α is Biot's coefficient, K is the drained bulk modulus of rock, K_i is the intrinsic bulk modulus of the solid constituent, and K_f is the bulk modulus of the pore fluid. The porosity of several intact samples of the Aar and Gamsboden granites was measured and found to be 0.007–0.009. The values of the other poro-elastic constants were based on those derived by Brace [44] for Westerly granite, which has a porosity of 0.01. Using values given by Brace of $\alpha = 0.45$, $K = 2.5\times10^{10}$ Pa, $K_i = 4.54\times10^{10}$ Pa, and $K_f = 0.24\times10^{10}$ Pa, the values of S_{si} for zero strain (Eq. 14a) and constant stress (Eq. 14b) boundary conditions are 1.4×10^{-7} m^{-1} and $2.2\times10^{-7}\,m^{-1}$, respectively, which are not greatly different. Using an S_{si} value of $1.8\times10^{-7}\,m^{-1}$ in Eq. (13) together with the range of hydraulic conductivity values of 3×10^{-12}–2×10^{-10} m/s gives corresponding estimates of diffusivity of 1.7×10^{-5}–$1.1\times10^{-3}\,m^2/s$. This compares to diffusivity values between 3×10^{-6} and $8\times10^{-6}\,m^2/s$ obtained from laboratory tests on an intact rock sample of Aar granite [1]. The diffusivity of the intact blocks was thus taken as 1×10^{-3}–$1\times10^{-5}\,m^2/s$. The corresponding times for 90% drawdown of pressure at the centre of the blocks were computed from Eq. (12) for a range of fracture spacings and are listed in Table 3. For a fracture spacing of 10 m (i.e. $L/2 = 5$ m), drawdown of pressure in the blocks and attendant contraction would be expected to occur on timescales of several hours to a month. This case would be appropriate if the meso-scale fractures have significant permeability, so that the effective block size is in accord with that shown in Fig. 9. The opposite case is when the meso-scale fractures are impermeable, so that the block size is determined by the spacing between water-bearing fault zones, which is 35 m on average and less than 100 m for most measured spacings. Hence a large fracture spacing of 100 m and an extremely low intact rock diffusivity of $1\times10^{-5}\,m^2/s$ results in a drawdown time of about 8 years. Given that the Gotthard highway tunnel was excavated approximately 20 years prior to the levelling measurements, it is reasonable to assume that complete drainage of pore pressure in the blocks bounding the drained fracture network had occurred by the time of the survey. Hence, in evaluating the effect of this drainage on the displacements using numerical models described in Part 2, steady state conditions were assumed to prevail.

Table 3
Time for pore-pressure drawdown at the centre of the intact crystalline blocks to reach 90% of the external drawdown as a function of diffusion distance (i.e. half-length, L, of the intact blocks) and their diffusivity, D_{si}

Diffusion distance (m)	Time (d)		
	$D_{si} = 1e{-}3\,m^2/s$	$D_{si} = 1e{-}4\,m^2/s$	$D_{si} = 1e{-}5\,m^2/s$
$L/2 = 5$	0.3	3	30
$L/2 = 10$	1.2	12	119
$L/2 = 20$	4.8	48	477
$L/2 = 50$	29.8	298	2980

5.3. Analytical assessment of consolidation above the Gotthard highway tunnel

The response of the fractured rock mass to progressive drainage is, in detail, very complicated, potentially involves all of the aforementioned elastic and inelastic deformation mechanisms. The detailed simulation of the response requires the numerical approaches described in Part 2. However, it is instructive to perform some analytic scoping calculations to evaluate the rock mass elastic properties required to explain the elastic component of compaction. The calculations are based on the solution to the problem of the vertical shortening of a horizontal layer of thickness, h, embedded in a porous medium resulting from an internal pore-pressure change within the layer under conditions of constant vertical stress and zero horizontal strain. The resulting estimate of subsidence is valid for situations

where pore-pressure drawdown occurs within a shallow, horizontal layer whose lateral dimensions are large compared to its thickness, which is less than 1 km for the case in question. For such a problem geometry it can be shown that the vertical strain, ε_{zz}, resulting from a drop in pore pressure, Δp, within a poro-elastic layer described by constants, α, K and v, is given by [33]

$$\Delta\varepsilon_{zz} = \frac{\alpha\Delta p}{3K}\frac{(1+v)}{(1-v)} \tag{15}$$

The vertical shortening across the layer in which the drawdown occurred can be computed from the vertical strain by multiplying by the layer thickness, h. Since the width of the layer is large compared to its depth, the vertical shortening should produce a surface subsidence of similar magnitude, at least near the centre of the trough. Thus, the expected subsidence at the surface, $u_z|_{z=0}$, is given by

$$\Delta u_z|_{z=0} = \frac{\alpha h\Delta p}{3K}\frac{(1+v)}{(1-v)} \tag{16}$$

Reasonable estimates for the drained Poisson's ratio and Biot's coefficient are given by the values for Westerly granite of $v = 0.25$, $\alpha = 0.45$. The greatest uncertainty applies to the layer thickness, h, the effective drained bulk modulus of the rock mass, K, and the average pore-pressure drawdown within the layer, Δp. Since the observed subsidence near the centre of the trough is known to be 12 cm, Eq. (16) can be rearranged to isolate the principal unknowns. Upon rearrangement, and substitution of $\Delta u = 12$ cm, $v = 0.25$, $\alpha = 0.45$, we have

$$\frac{K}{h\Delta p} = 2.1 \tag{17}$$

An upper bound on K for the layer is given by the drained bulk modulus of the intact blocks (i.e. neglecting the effects of fractures), which was taken as 25 GPa by analogy with the value for Westerly granite. The bulk modulus estimates obtained from uniaxial compression tests on three samples from the Aar and Gamsboden granite range between 18 and 23 GPa [1]. Similarly, an upper bound on the mean drawdown is given by the pre-excavation pore pressure averaged over the entire depth interval, which would be ~5 MPa (i.e. total drainage of a 1000 m high water saturated rock mass). Thus, if the rock mass had an elastic modulus appropriate for intact granite, an extreme 5 MPa drawdown would require a layer thickness of 2380 m to produce the observed subsidence. This is clearly untenable, since the maximum overburden is 1500 m. Adopting more realistic values for mean drawdown of 2.5 MPa and drawdown layer thickness of 1000 m implies that the effective drained bulk modulus of the layer is 5.25 GPa, which is a factor of four lower than the value for intact granite. This result highlights the impact of fractures in reducing the effective modulus of the rock mass. The meso-scale fractures have the greatest effect in reducing the stiffness of the rock mass to vertical loading since they include a sub-horizontal set, at least near the surface. These horizontal fractures effectively dissect the medium into an assemblage of blocks whose average size is a few metres at most (Fig. 9). To determine the normal stiffness that must be ascribed to these fractures in order to explain the reduction in bulk modulus from intact values, K_b, to large-scale values, K_m, we consider the intact blocks to form a regular cubic lattice of spacing, d_f. The required constant normal stiffness of the fractures can then be computed from the relation:

$$k_n = \frac{3}{d_f}\left(\frac{1}{K_m} - \frac{1}{K_b}\right)^{-1} \tag{18}$$

Taking K_b as 25 GPa and d_f as 1–10 m (Fig. 9) implies that a fracture normal stiffness of 20–2 MPa/mm, respectively, is required to give an effective rock mass bulk modulus of $K_m = 5.25$ GPa. Such values correspond to relatively compliant fractures that are usually found in the near-surface. However, it is probable that the elastic moduli of the "intact" blocks themselves would be somewhat lower than values measured in laboratory tests owing to the presence of a class of cracks and imperfections whose scales are larger than core size. A discussion of the scale effect and sample disturbance is beyond the scope of this study. It suffices to conclude that the subsidence data indicate the modulus of the rock mass is substantially less than values typically measured on granite core, and that this is at least in part due to the meso-scale fractures. In Part 2 we will develop the investigation further to include other mechanisms that could contribute to subsidence.

6. Discussion and conclusions

Surface settlement due to consolidation of a rock mass, whether through fluid extraction or tunnel drainage, is generally associated with loosely consolidated sediments or high porosity rocks. The present observations indicate that significant subsidence can also occur through consolidation processes in crystalline rock masses in which pore pressure is lowered. The subsidence measured along the Gotthard pass was observed after the construction of the Gotthard highway tunnel, and coincides spatially with a 3 km section of the tunnel where it passes through a geological unit, the Gamsboden granite gneiss, that contained faults which produced large initial inflows of water when perforated. Thus, drawdown of pore pressure within the unit and attendant consolidation processes appears to be responsible for the subsidence.

Several possible hydro-mechanically coupled mechanisms might account for the observed surface settlements. An important geological factor in this regard is that the dominant structures are steeply inclined faults that strike sub-perpendicular to the tunnel axis. These faults have a mean spacing of 35 m over the 3 km section where they produce the large initial inflows, and provide conduits for rapid, deep penetration of drainage into the rock mass.

Closure of these high-angle faults in response to reduced internal pressure would produce vertical compaction of the rock mass only indirectly through a Poisson's ratio effect, and thus would not be very effective in generating subsidence. A more important contribution to the settlement is likely to come from the eventual drawdown of pore pressure within the rock volumes between the fault zones. Mapping studies indicate that these volumes are dissected into blocks of mean side length of a couple of metres by several sets of meso-scale fractures that are present within the Gamsboden unit. The time required for pore-pressure drawdown to penetrate the rock volumes from the faults is almost certainly governed by the hydromechanical properties of these meso-scale fractures, about which little is known. Estimates of approximate equilibration time for the intact blocks range from several days to 8 years. For pressure diffusion within the fault zones, best estimates for diffusion times between tunnel and ground surface is in the range 8 h to 165 days. Since both these time constants are small compared to the 28 years that had elapsed since tunnel excavation when the 1998 level survey that revealed the subsidence was performed, it is likely that almost complete equilibration of the drawdown in the faults with the pore pressure in the rock mass between them had occurred by this time. The compaction accompanying the drawdown of the rock volume is primarily dependent upon the effective elastic bulk modulus of the volume, which is influenced by the normal-stiffness properties of the meso-scale fractures and the bulk modulus of the blocks they bound. Explaining the entire 12 cm of measured subsidence by the elastic compaction mechanism would require either unusually compliant fractures or a lower bulk modulus for the "intact" blocks that is atypical of values measured on core samples. As is concluded from the detailed modelling of these data presented in Part 2, it is most probable that several mechanisms described earlier acted in concert, including inelastic shear deformation.

If these findings are correct, they suggest that consolidation of a fractured crystalline rock mass through deep tunnel drainage can result in surface settlements that are of sufficient magnitude to pose a potential threat to the integrity of any nearby large concrete structures such as thin arch dams. This is a conclusion of considerable importance given that four deep rail tunnels are currently under construction through the Alps.

Acknowledgements

The authors would like to thank the maintenance team of the Gotthard highway tunnel for their kind support of this work and the AlpTransit Gotthard AG for the permission to publish the settlement data. Thanks are also extended to Dr. Giovanni Lombardi (Lombardi SA, Engineering Consultants) for his input and discussions.

Appendix A

There are few published studies pertaining to the normal stiffness of brittle fault zones. Martin et al. [45] reported values for a brittle fault zone consisting of fractures, fault breccias and clay-gouge in the Lac du Bonnet granite batholith at the Underground Research Laboratory (URL)-test site in Canada. They report values of 2–6 MPa/mm for a highly compliant cataclastic zone (i.e. crushed and broken with clay gouge) where the normal stiffness measurements were recorded under low effective normal stresses between 0.5 and 1.4 MPa. In contrast, *in situ* normal stiffness values approximately an order of magnitude higher were measured across two granite-hosted ductile shear zones overprinted by minor brittle deformation at the Grimsel Rock Laboratory in central Switzerland [46]. Unfortunately, no direct measurements of normal stiffness were made across the fault zones and meso-scale fractures encountered in the Gotthard safety tunnel. Thus, estimates were calculated from published values of the elastic modulus of fault gouge and the normal stiffness of single unfilled joints. The water-bearing fault zones observed in the safety tunnel consist of multiple fractures usually filled with gouge. Laboratory tests on fault gouge material yielded Young's modulus estimates of 0.1–1.5 GPa [1,47–49]. Given that the *in situ* effective normal stress is likely to be of the order of 10–15 MPa, a lower limit on the Young's modulus of the gouge of 0.5 GPa was adopted. The thickness of individual brittle fault zone cores mapped in the tunnel ranges from centimetres to metres, with 98% having thicknesses of $\leqslant 1$ m [1,14,15]. Thus, taking thickness as 1 m places a lower bound on the normal stiffness of a single gouge-filled fracture of 0.5 MPa/mm.

The value of normal stiffness of individual fractures without gouge was estimated from an extensive literature survey reported in [37]. According to the a semi-logarithmic closure law, the normal stiffness behaviour of an unfilled fracture is completely defined by a single parameter, referred to by Evans et al. [50] as the "stiffness characteristic". Based on this literature study [37], stiffness characteristic values range from 720 mm^{-1} for well-mated fractures in laboratory tests to 3 mm^{-1} for *in situ* tests on a fracture intersected in a borehole in granite [51]. We consider the latter value to be more representative of the fractures present in the fault zones encountered along the tunnel. A fracture with a stiffness characteristic value of 3 mm^{-1} under an effective normal stress of 10 MPa would have a normal stiffness of 30 MPa/mm. A fault zone that consisted of 10 such gouge-free fractures would have a stiffness of 3 MPa/mm and one with 100 fractures would have 0.3 MPa/mm, comparable with a fracture filled with 1 m of gouge. Based upon these considerations, we adopt a range of values for the normal stiffness of the brittle fault zones encountered in the Gotthard safety tunnel of 0.5–30 MPa/mm.

References

[1] Zangerl C. Analysis of surface subsidence in crystalline rocks above the Gotthard highway tunnel, Switzerland. PhD thesis, ETH Zurich; 2003. 190p.

[2] Schmidt B. Consolidation settlement due to soft ground tunneling. In: Proceedings of the 12th international conference on soil mechanics and foundation engineering, Rio de Janeiro, vol. 2. Rotterdam: Balkema; 1989. p. 797–800.

[3] Karlsrud K, Sander L. Subsidence problem caused by rock-tunnelling in Oslo. In: Saxena SK, editor. International conference on evaluation and prediction of subsidence. New York: American Society of Civil Engineers; 1979. p. 197–213.

[4] Lombardi G. The FES rock mass model—part 2: some examples. Dam Eng 1992;3(3):201–21.

[5] Lombardi G. Les tassements exceptionnels au barrage de Zeuzier. Pub Soc Mécan Sols Roches 1988;118:39–47 (in French).

[6] Poland JF. Subsidence in United States due to ground-water withdrawal. J Irrig Drain Div ASCE 1981;107(IR2):115–35.

[7] Allis RG. Review of subsidence at Wairakei field, New Zealand. Geothermics 2000;29(4–5):455–78.

[8] Geertsma J. Land subsidence above compacting oil and gas reservoirs. J Pet Technol 1973;25:734–44.

[9] Kahle H-G, Geiger A, Bürki B, Gubler E, Marti U, Wirth B, et al. Recent crustal movements, geoid and density determination: contribution from integrated satellite and terrestrial measurements. In: Pfiffner OA, et al., editors. Deep structure of the Swiss Alps: results of NRP 20. Basel: Birkhäuser; 1997. p. 251–9.

[10] Michalski I, Soom M. The Alpine thermo-tectonic evaluation of the Aar and Gotthard massifs, central Switzerland: fission-track ages on Zirkon and Apetite and K–Ar mica ages. Schweiz Mineral Petrogr Mitt 1990;70:373–87.

[11] Salvini D. Deformationsanalyse im Gotthardgebiet. Report by the Institute of Geodesy and Photogrammetry (ETH Zurich), Zurich, Report #297; 2002. 27p. (ISBN: 3906467341).

[12] Labhart TP. Aarmassiv, Gotthardmassiv und Tavetscher Zwischenmassiv: Aufbau und Entstehungsgeschichte. In: Löw, Wyss, editors. Vorerkundung und Prognose der Basistunnel am Gotthard und am Lötschberg, Tagungsband zum Symposium Geologie AlpTransit Zurich. Rotterdam: Balkema; 1999. p. 31–43.

[13] Zangerl C, Loew S, Eberhardt E. Structure, geometry and formation of brittle discontinuities in anisotropic crystalline rocks of the Central Gotthard Massif, Switzerland. Eclogae Geol Helv 2006;99:271–90.

[14] Schneider TR. Gotthard Strassentunnel—Geologischer Schlussbericht Nordseite II Geologie. 305am II 3a-4. Unpublished report, available at the Kantonsbibliothek Uri, 6460 Altdorf UR, Schweiz; 1979.

[15] Wanner H. Galeria Stradale del San Gottardo, Rapporto Finale Lotto Sud—Prohilo Geologico attraverso il tunnel di sicurezza del Gottardo. Unpublished report, available at the Kantonsbibliothek Uri, 6460 Altdorf UR, Schweiz; 1982.

[16] Zangerl C, Eberhardt E, Loew S. Ground settlements above tunnels in fractured crystalline rock: numerical analysis of coupled hydro-mechanical mechanisms. Hydrogeol J 2003;11(1):162–73.

[17] Wang H, Latham J-P, Poole AB. In-situ block size assessment from discontinuity spacing data. In: Price DG, editor. Proceedings of the 6th International IAEG Congress. Rotterdam: Balkema; 1990. p. 117–27.

[18] Lu P, Latham J-P. Developments in the assessment of in-situ block size distributions of rock masses. Rock Mech Rock Eng 1999; 32(1):29–49.

[19] Luetzenkirchen VH. Structural geology and hydrogeology of brittle fault zones in the central and eastern Gotthard massif, Switzerland. PhD thesis, ETH Zurich; 2003. 264p.

[20] Jacob CE, Lohman SW. Nonsteady flow to a well of constant drawdown in an extensive aquifer. Trans AGU 1952;33:559–69.

[21] Löw S, Ehrminger B, Klemenz W, Gilby D. Abschätzung von Bergwasserzuflüssen ond Oberflächenauswirkungen am Beispiel des Gotthard-Basistunnels. In: Oddsson B, editor. Instabile Hänge und andere riskorelevante natürliche Prozesse, Proceedings of the Centro Stefano Franciscini Ascona. Basel: Birkhäuser; 1996. p. 353–76.

[22] Robin P-YF. Note on effective pressure. J Geophys Res 1973; 78(14):2434–7.

[23] Bandis SC, Lumsden AC, Barton NR. Fundamentals of rock joint deformation. Int J Rock Mech Min Sci 1983;20(6):249–68.

[24] Sun Z, Gerrad C, Stephansson O. Rock joints compliance tests for compression and shear loads. Int J Rock Mech Min Sci 1985;22(4): 197–213.

[25] Plesha ME. Constitutive models for rock discontinuities with dilatancy and surface degradation. Int J Numer Anal Meth Geomech 1987;11(4):345–62.

[26] Zimmerman RW, Bodvarsson GS. Hydraulic conductivity of rock fractures. Transp Porous Media 1996;23:1–30.

[27] Esaki T, Du S, Mitani Y, Ikusada K, Jing L. Development of a shear-flow test apparatus and determination of coupled properties for a single rock joints. Int J Rock Mech Min Sci 1999;36:641–50.

[28] Chen Z, Narayan SP, Yang Z, Rahman SS. An experimental investigation of hydraulic behaviour of fractures and joints in granitic rock. Int J Rock Mech Min Sci 2000;37:1061–71.

[29] Renshaw CE. On the relationship between mechanical and hydraulic apertures in rough-walled fractures. J Geophys Res 1995;100(B12): 24629–36.

[30] Biot MA. General theory of three-dimensional consolidation. J Appl Phys 1941;12:155–64.

[31] Nur A, Byerlee JD. An exact effective stress law for elastic deformation of rock with fluids. J Geophys Res 1971;76(26):6414–9.

[32] Detournay E, Cheng AHD. Fundamentals of poroelasticity. In: Hudson JA, editor. Comprehensive rock engineering, vol. 1. Oxford: Pergamon; 1993. p. 113–71.

[33] Wang HF. Theory of linear poroelasticity with applications to geomechanics and hydrogeology. Princeton: Princeton University Press; 2000. 276p.

[34] Jacob CE. Effective radius of drawdown test to determine artesian well. Proc Am Soc Civ Eng 1946;72(5):629–46.

[35] Ofterdinger US. Ground water flow systems in the Rotondo granite, Central Alps (Switzerland). PhD thesis, ETH Zurich; 2001. 198p.

[36] Doe TW, Long JCS, Endo HK, Wilson CR. Approaches to evaluating the permeability and porosity of fractured rock masses. In: Goodman R, Heuze F, editors. Proceedings of the 23rd US Symposium on Rock Mechanics. New York: Society of Mining Engineers; 1982. p. 30–8.

[37] Zangerl C, Evans KF, Eberhardt E, Loew S. Normal stiffness of fractures in granitic rock: a compilation of laboratory and in-situ experiments. Int J Rock Mech Min Sci; 2008, doi:10.1016/j.ijrmms.2008.02.001.

[38] Rutqvist J, Noorishad J, Tsang C-F, Stephansson O. Determination of fracture storativity in hard rocks using high-pressure injection testing. Water Resour Res 1998;34(10):2551–60.

[39] Kessels W, Kück J. Hydraulic communication in crystalline rock between the two boreholes of the Continental Deep Drilling Project in Germany. Int J Rock Mech Min Sci 1995;32(1):37–47.

[40] Evans K, Dahlø T, Roti J-A. Mechanisms of pore pressure–stress coupling which can adversely affect stress measurements conducted in deep tunnels. Pure Appl Geophys 2003;160(5–6):1087–102.

[41] Brace WF. Permeability of crystalline and argillaceous rocks. Int J Rock Mech Min Sci 1980;17(5):241–51.

[42] Vomvoris S, Frieg B, Bossart P, Gmünder C, Heiniger P, Jacquet O, Watanabe K. Grimsel test site—overview of Nagra field and modelling activities in the ventilation drift (1988–1990). Report # NTB91-34, NAGRA (National Cooperative for the Disposal of Radioactive Waste), Wettingen; 1992. 92 p.

[43] Evans K, Beavan J, Simpson D, Mousa S. Estimating aquifer parameters from analysis of forced fluctuations in well level: an example from the Nubian Formation near Aswan, Egypt, 3. Diffusivity estimates for saturated and unsaturated zones. J Geophys Res 1991;96(B7):12161–91.

[44] Rice JR, Cleary MP. Some basic stress diffusion solutions for fluid-saturated elastic porous media with compressible constituents. Rev Geophy Space Phys 1976;14(2):227–41.

[45] Martin CD, Davison CC, Kozak ET. Characterizing normal stiffness and hydraulic conductivity of a major shear zone in granite. In: Barton N, Stephansson O, editors. Proceedings of the International Symposium on Rock Joints. Rotterdam: Balkema; 1990. p. 549–56.

[46] Majer EL, Myer LR, Peterson Jr, JE, Karasaki K, Long JCS, Martel SJ, et al. Joint seismic, hydrogeological and geomechanical investigations of a fracture zone in the Grimsel Rock Laboratory, Switzerland. Report # NTB90-49, NAGRA (Swiss National Cooperative for Radioactive Waste Disposal), Wettingen; 1990. 180p.

[47] Laws S, Eberhardt E, Loew S, Descoeudres F. Geomechanical properties of shear zones in the Eastern Aar Massif, Switzerland and their implication on tunnelling. Rock Mech Rock Eng 2003; 36(4):271–303.

[48] Kovari K, Vogelhuber M. Triaxiale Druckversuche im Labor, Sondierbohrung SB3.2, AlpTransit Gotthard Basistunnel. Internal report, Institut für Geotechnik, ETH Zurich; 1998.

[49] Habimana J, Labiouse V, Descoeudres F. Geomechanical characterisation of cataclastic rocks: experience from the Cleuson–Dixence project. Int J Rock Mech Min Sci 2002;39(6):677–93.

[50] Evans KF, Kohl T, Rybach L, Hopkirk RJ. The effects of fracture normal compliance on the long term circulation behaviour of a hot dry rock reservoir: a parameter study using the new fully-coupled code FRACTure. Trans Geotherm Resour Counc 1992;16:449–56.

[51] Jung R. Hydraulic *in situ* investigations of an artificial fracture in the Falkenberg Granite. Int J Rock Mech Min Sci 1989;26(3–4):301–8.